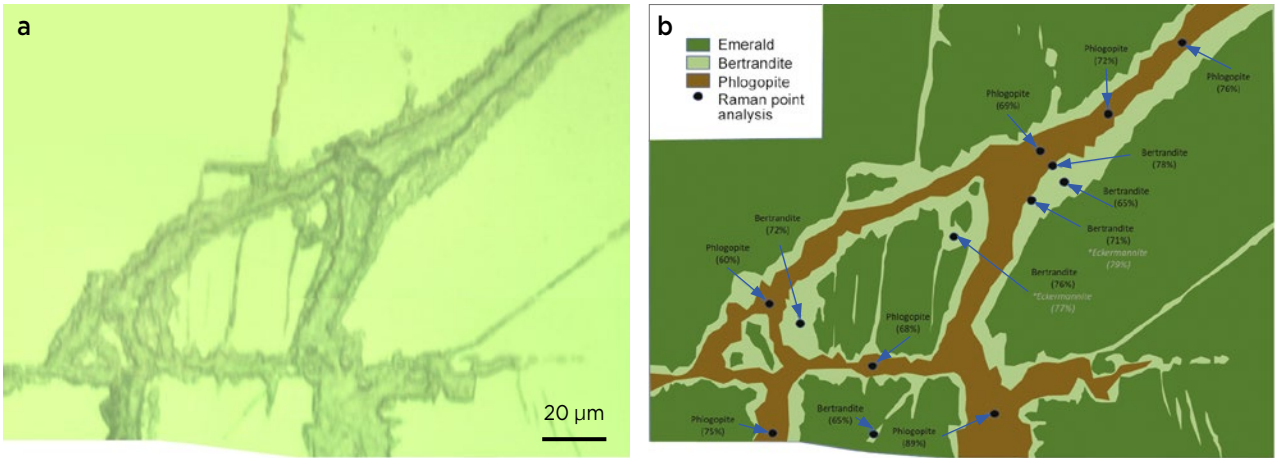

Figure 3: (**a**) This reflected-light image of the studied area of the emerald, as seen with the Raman microscope, shows tonal variations corresponding to different domains that are present. (**b**) A mineral map of this area depicts the relationship among the various phases: the emerald host, a bertrandite-bearing alteration zone and a fissure network filled by phlogopite. In parentheses are the 'match percentages' obtained for each Raman analysis point. Photomicrograph and diagram by R. Zellagui.

Based on our observations, we propose that after the emerald crystallised, a late-stage fluid entered the fissures and induced an alteration halo by transforming the emerald host into the bertrandite-bearing assemblage, and this was accompanied by the formation of phlogopite along the open fissures. The use of both reflected light at high magnification and Raman micro-spectroscopy were necessary for differentiating the various mineral phases present and their spatial and temporal relationships in the studied emerald.

Dr Riadh Zellagui (riadh@aglgemlab.com)
American Gemological Laboratories
New York, New York, USA

References

Araújo Neto, J.F. de, Barreto, S. de B., Carrino, T.A., Müller, A. & Santos, L.C.M. de L. 2019. Mineralogical and gemological characterization of emerald crystals from Paraná deposit, NE Brazil: A study of mineral chemistry, absorption and reflectance spectroscopy and thermal analysis. *Brazilian Journal of Geology*, **49**(3), article e20190014 (15 pp.), https://doi.org/10.1590/2317-4889201920190014.

Barton, M.D. & Young, S. 2002. Non-pegmatitic deposits of beryllium: Mineralogy, geology, phase equilibria and origin. *In*: Grew, E.S. (ed) *Beryllium*. Mineralogical Society of America, Washington DC, USA, 591–692, https://doi.org/10.1515/9781501508844-015.

Colombo, F., Rinaudo, C. & Trossarelli, C. 2000. The mineralogical composition of maw-sit-sit from Myanmar. *Journal of Gemmology*, **27**(2), 87–92, https://doi.org/10.15506/JoG.2000.27.2.87.

Giuliani, G., Groat, L.A., Marshall, D., Fallick, A.E. & Branquet, Y. 2019. Emerald deposits: A review and enhanced classification. *Minerals*, **9**(2), article 105 (63 pp.), https://doi.org/10.3390/min9020105.

Harlow, G.E. & Sorensen, S.S. 2001. Jade: Occurrence and metasomatic origin. *Australian Gemmologist*, **21**(1), 7–11.

Lederer, G.W., Foley, N.K., Jaskula, B.W. & Ayuso, R.A. 2016. *Beryllium—A Critical Mineral Commodity—Resources, Production, and Supply Chain*. U.S. Geological Survey, Reston, Virginia, USA, 4 pp.

Oberti, R., Boiocchi, M., Hawthorne, F.C., Ball, N.A. & Harlow, G.E. 2015. Eckermannite revised: The new holotype from the jade mine tract, Myanmar—Crystal structure, mineral data, and hints on the reasons for the rarity of eckermannite. *American Mineralogist*, **100**(4), 909–914, https://doi.org/10.2138/am-2015-5132.

Cinnabar Inclusions in Ethiopian Opal

The authors recently examined a 15.8 ct Ethiopian opal (Figure 4) that contained numerous red dendritic particles that each measured up to 70–100 µm in diameter (Figure 5). The Ethiopian origin of the opal was confirmed by its physical properties (slight hydrophane character and rounded columnar structure) and its chemical composition (high Ba concentration; Rondeau *et al.* 2010). The inclusions were identified by Raman micro-spectroscopy as cinnabar (HgS). Energy-dispersive X-ray fluorescence (EDXRF) chemical analyses of

Figure 4: This 15.8 ct opal from Ethiopia was examined for this report. Photo by C. Caplan.

the top surface of the sample confirmed the presence of Hg and S. Cinnabar and opal are associated in numerous localities, particularly in the western USA (Knopf 1915; Gettens *et al.* 1972; https://www.mindat.org/min-3004.html). However, cinnabar is only rarely mentioned as inclusions in opal (see, e.g., Gaillou 2015). Also known is an opalised or silicified cinnabar material known as myrickite, in which the high concentration of cinnabar inclusions induces an intense orange or red colour (Manutchehr-Danai 2009; Melero *et al.* 2019).

To the authors' knowledge, this is the first time that cinnabar inclusions have been documented in opal from Ethiopia. Their dendritic habit suggests relatively fast growth, whereas magnetite inclusions reported in Ethiopian opal have a well-formed octahedral habit (Rondeau *et al.* 2010), suggesting slow growth. This points to a vast domain of parameters possible (at least in terms of growth rate and chemistry) for the formation of inclusions in Ethiopian opal, which perhaps reflects the expansive region over which those deposits occur.

Féodor Blumentritt[1] (feodor.blumentritt@ggtl-lab.org), Candice Caplan[1], Emmanuel Fritsch FGA[2] and Franck Notari[1]
[1]GGTL Laboratories Switzerland, Geneva, Switzerland
[2]IMN-CNRS and University of Nantes, France

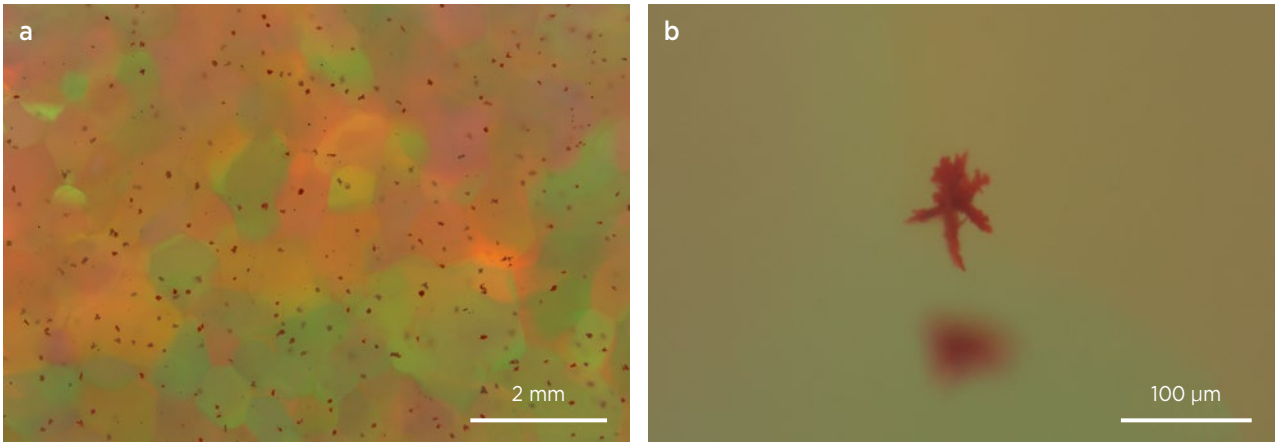

Figure 5: (**a**) The opal contains red cinnabar inclusions across the top surface of the cabochon. (**b**) A closer look at one of these inclusions shows its dendritic form. Photomicrographs by F. Notari.

References

Gaillou, E. 2015. An overview of gem opals: From the geology to color and microstructure. *Thirteenth Annual Sinkankas Symposium—Opal*, Carlsbad, California, USA, 18 April, 10–19.

Gettens, R.J., Feller, R.L. & Chase, W.T. 1972. Vermilion and cinnabar. *Studies in Conservation*, **17**(2), 45–69, https://doi.org/10.2307/1505572.

Knopf, A. 1915. Some cinnabar deposits in western Nevada. *Contributions to Economic Geology, 1915. Part I. Metals and Nonmetals Except Fuels*, U.S. Geological Survey Bulletin 620, 59–68, https://pubs.usgs.gov/bul/0620d/report.pdf.

Manutchehr-Danai, M. 2009. *Dictionary of Gems and Gemology*. Springer, Berlin and Heidelberg, Germany, 1,037 pp., https://doi.org/10.1007/978-3-540-72816-0.

Melero, D., Lobato, B., López-Antón, M.A. & Martínez-Tarazona, M.R. 2019. Identification of mercury species in minerals with different matrices and impurities by thermal desorption technique. *Environmental Science and Pollution Research*, **26**(11), 10867–10874, https://doi.org/10.1007/s11356-019-04245-8.

Rondeau, B., Fritsch, E., Mazzero, F., Gauthier, J.-P., Cenki-Tok, B., Bekele, E. & Gaillou, E. 2010. Play-of-color opal from Wegel Tena, Wollo Province, Ethiopia. *Gems & Gemology*, **46**(2), 90–105, https://doi.org/10.5741/gems.46.2.90.

Violet Spinel with Strong Green Fluorescence

Recently submitted to Stone Group Laboratories by gem dealer John Bachman was a 3.73 ct marquise-cut spinel showing light violet ('lilac') colouration (Figure 6a). It was cut from a rough parcel that he had acquired more than 30 years ago from Okkampitiya, Sri Lanka. Of note was its strong, bright bluish green fluorescence to long-wave UV excitation (Figure 6b), since most gem spinel is either inert (due to the presence of Fe) or fluoresces red (due to Cr or Co).

The stone's identity as spinel was confirmed by Raman analysis using a Magilabs GemmoRaman-532SG instrument. Its RI was 1.713 and hydrostatic SG was 3.56. The relatively low RI eliminated the possibility of it being a Verneuil-grown (flame-fusion) synthetic spinel. Between crossed polarisers, anomalous extinction was seen rolling across the stone while it was rotated. Only a very faint magnetic susceptibility was detected using the float method. The stone was eye-clean, and microscopic examination revealed only one small 'fingerprint' and some surface features: a 'natural' on the girdle and what appeared to be a surface-reaching fissure or stress crack.

EDXRF spectroscopy was performed with an Amptek X123-SDD spectrometer (Figure 7). Although significant Fe was present, Mn was also found in an unusually high concentration for spinel. Also detected were Zn, Ni and Ga. The presence of Ga confirmed the natural origin of this stone (which the unusual fluorescence had initially called into doubt).

Ultraviolet-visible-near infrared (UV-Vis-NIR) spectroscopy (Figure 8) with a Magilabs GemmoSphere unit revealed absorption features resembling those recorded by Kammerling & Fritsch (1991) for a similar-coloured lilac spinel that showed somewhat weaker green fluorescence. Most prominent were absorption peaks at 555, 576 and 620 nm related to Co^{2+} (cf. Belley & Palke 2021). (Although no Co was found with EDXRF analysis, this element is often below the detection limit of our instrument and is frequently masked by or merged with the *K*α or *K*β peaks of adjacent elements.) The absorption spectrum also showed Fe-related peaks in the 375–478 nm range, and a sharp, distinct peak at 427 nm attributed to Mn^{2+} (cf. Schmetzer *et al.* 1989). We infer that the presence of Fe^{2+} and Fe^{3+} with traces of Co^{2+} in tetrahedral coordination is responsible for the lilac (violet) body colour of this spinel.

To compare the green fluorescence of this stone to a spinel showing more common red luminescence, fluorescence spectroscopy was performed with a Magilabs EXA spectrometer (Figure 9). The emission peak of the lilac spinel's green fluorescence was centred at about 510 nm. By contrast, the red spinel's red fluorescence produced a series of luminescence peaks that were centred around 700 nm. Green fluorescence in spinel is attributed to tetrahedral Mn^{2+} (Kammerling & Fritsch 1991; Sehgal &

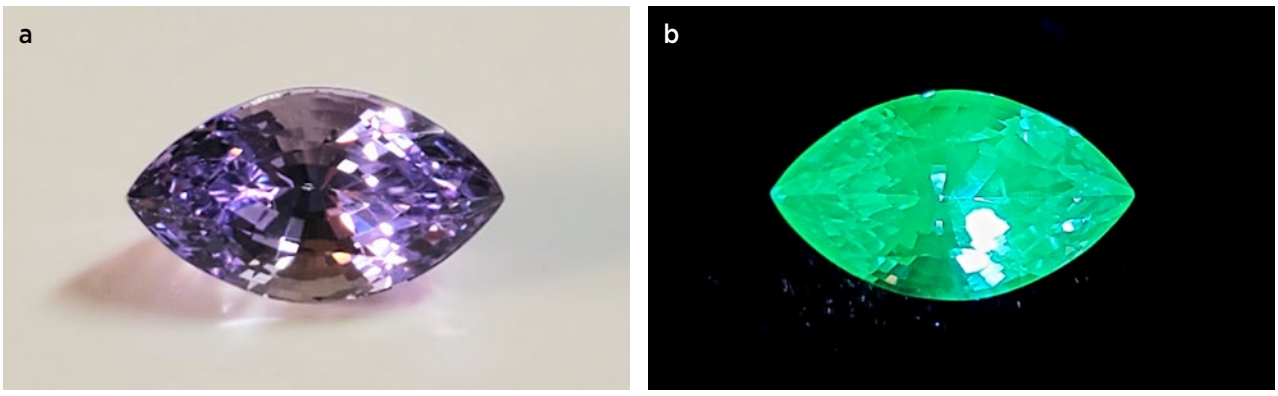

Figure 6: (**a**) This 'lilac' spinel from Sri Lanka weighs 3.73 ct and measures 12.64 × 7.22 × 6.52 mm. (**b**) Viewed under long-wave (369 nm LED) UV radiation, the spinel emits an unusual strong bluish green luminescence. Photos by C. Williams.